Performance of the Multiband Imaging Photometer for SIRTF

G. H. Rieke[a]. E. T. Young[a], P. A. R. Ade[b], J. W. Beeman[c], W. Burmester[d], J. Cadien[a], K. A. Ennico[a], K. D. Gordon[a], M. Hegge[d], G. B. Heim[d], M. L. Henderson[d], T. Horne[a], D. M. Kelly[a], T. J. McMahon[a], M. Neitenbach[d], A. Noriega-Crespo[e], G. Rivlis[a], R. Schnurr[a], J. P. Schwenker[d], S. Siewert[d], J. A. Stansberry[a], D. W. Strecker[d], G. S. Winters[a], and C. Yanoski[d]

[a] Steward Observatory, University of Arizona, Tucson, AZ 85721
[b]Queen Mary and Westfield College, Mile End Road, London E1 4NS
[c]Berkeley National Laboratory, M/S 2-200, 1 Cyclotron Rd., Berkeley, CA 94720
[d]Ball Aerospace & Technologies Corp, P. O. Box 1062, Boulder, CO 80306-1062
[e]SIRTF Science Center, 770 S. Wilson Ave., Pasadena, CA 91125

ABSTRACT

We describe the test approaches and results for the Multiband Imaging Photometer for SIRTF (MIPS). To verify the performance within a "faster, better, cheaper" budget required innovations in the test plan, such as heavy reliance on measurements with optical photons to determine instrument alignment, and use of an integrating sphere rather than a telescope to feed the completed instrument at its operating temperature. The tests of the completed instrument were conducted in a cryostat of unique design that allowed us to achieve the ultra-low background levels the instrument will encounter in space. We controlled the instrument through simulators of the mission operations control system and the SIRTF spacecraft electronics, and used cabling virtually identical to that which will be used in SIRTF. This realistic environment led to confidence in the ultimate operability of the instrument. The test philosophy allowed complete verification of the instrument performance and showed it to be similar to pre-integration predictions and to meet the instrument requirements.

Keywords : infrared, integration and test, astronomical instrumentation

1. INTRODUCTION

The Multiband Imaging Photometer for SIRTF (MIPS) is the far infrared instrument for this mission. Central to its operation is the first true imaging array for the far infrared, with 32x32 pixels of Ge:Ga, used for low resolution spectroscopy from 53 to 100μm and for imaging at 70μm. The instrument also uses a high performance 128x128 pixel Si:As BIB detector array operating at 24μm and a 40 pixel stressed Ge:Ga array operating at 160μm. These devices are integrated into a compact optical design that allows imaging in 5 arcmin fields and feeds both a high magnification mode for 70μm imaging and the 53 – 100μm spectrometer with a single mechanism, a cryogenic scan mirror.

The design of the MIPS is summarized in Figure 1. Radiation is intercepted near the telescope focal plane by two pickoff mirrors and reflected into the instrument. Two distinct optical trains are used, one for the functions between 50 and 100μm and the other for the 24 and 160μm imaging. In each optical train, the light from the pickoff mirror reflects off a Fabry mirror near the back of the instrument that forms a pupil on the appropriate mirror facet on the cryogenic scan mirror mechanism (CSMM). The surrounds of the scan mirror facets are carefully blackened to act as Lyot stops to limit the instrument response to stray light. Light reflected by the 70μm scan mirror facet can be directed into three optical trains, corresponding to large field imaging, high magnification imaging (the plate scale is decreased by a factor of two), and spectroscopy. Although the wavefronts from these optical trains approach the detector array from different angles, the depth of focus is sufficiently large that there is no measurable image degradation. The other optical train first forms a re-imaged focal plane, where the 24 and 160μm fields are separated. Each is then re-imaged onto the appropriate detector array. A reimaged pupil is placed just in front of each detector array, where a baffle is placed to further limit stray radiation. In addition to switching among the 70μm optical trains, the scan mirror is used to move the field of view on the sky, allowing dithering compact sources on the arrays, chopping large ones against neighboring sky, and efficient mapping. In the latter operation, the telescope is tracked at a constant rate and the images are frozen on the arrays by driving the scan mirror in a sawtooth that counters the telescope motion. An additional important feature of the

instrument is a set of reverse bolometer thermal emitters or calibration stimulators that are to be flashed periodically while data are obtained to track the calibration of the far infrared arrays.

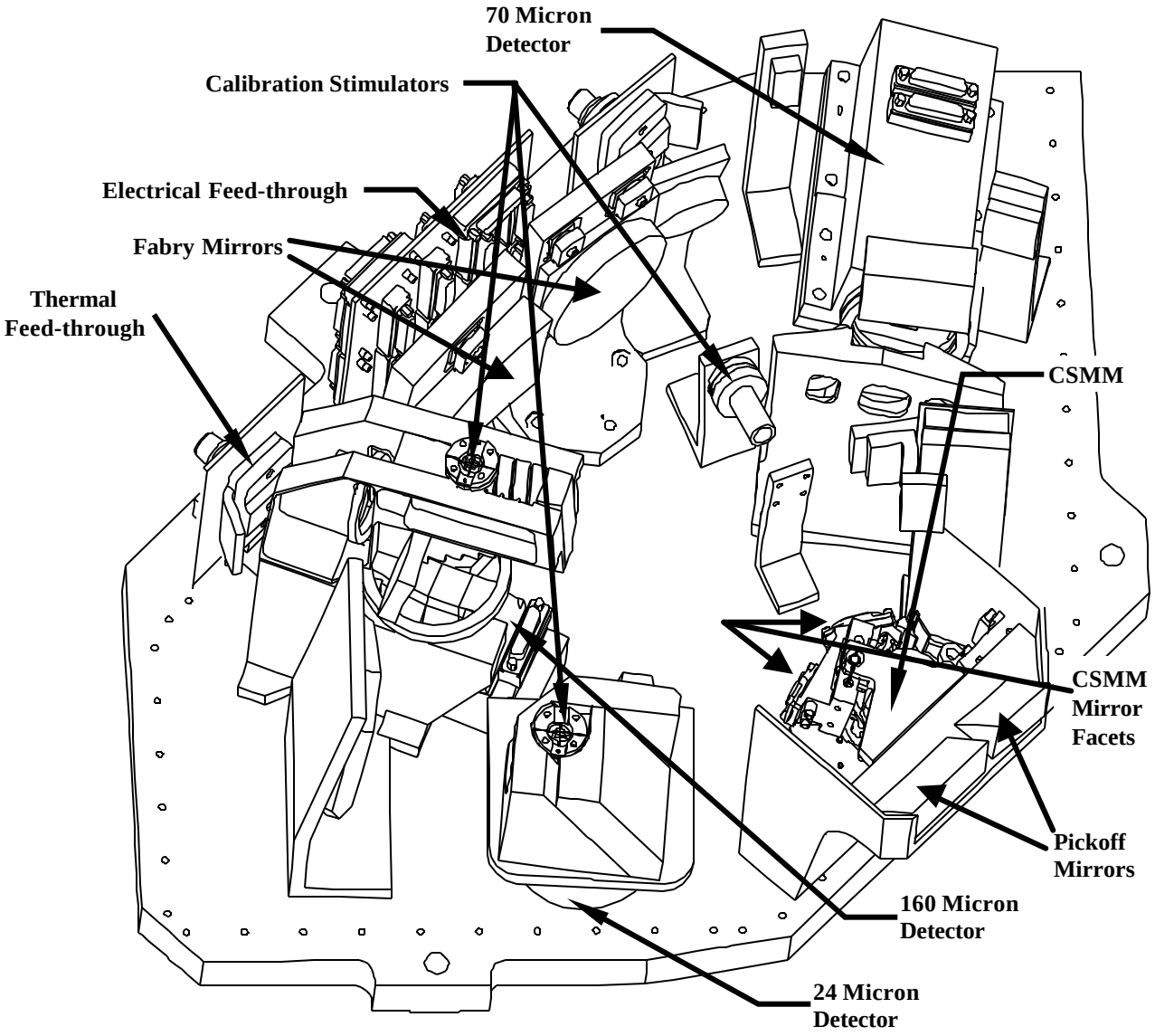

Figure 1. - The MIPS Cold Instrument Assembly.

Further description of the design of MIPS can be found in Heim et al.[1] The detector arrays described in van Cleve et al.[2] (24μm); Young et al.[3] (70μm); and Schnurr et al.[4] (160μm). The scan mirror is described in Warden and Heim[5].

The SIRTF payload was built to an accelerated schedule and with a smaller budget than had become customary for ambitious general purpose astronomical instruments. In addition, the long wavelength of operation presented opportunities and challenges in the integration and test of MIPS. This paper discusses the approaches used to assemble and test the instrument, and it compares the measured performance with the design expectations.

2. MIPS OPTICAL SYSTEM ALIGNMENT

The integration of the instrument optics presented the following issues:

1. Proper operation requires a high performance cryogenic system to hold the 160μm array heat sink below 1.5K.
2. It was expected (and later confirmed by experience during testing) that such a cryogenic system would require at least two weeks to warm up the instrument, open the vacuum vessel, make a simple adjustment, renew the vacuum, and cool down to proper operating temperature.
3. The saturation limits of the arrays, combined with the huge infrared backgrounds from normal room temperature environments, dictated that the cryostat be operated as a closed system, i.e., without a window but with all necessary test sources and optics within the photon-tight cold space
4. Measurement of alignments would be compromised by diffraction at the instrument operating wavelengths
5. The far infrared detector arrays were the biggest technical challenge in the instrument, and we wanted to delay their integration into the instrument to minimize schedule risk and the possibility of damaging them in an accident.

On the other hand, given the long wavelengths of operation, the alignment was more forgiving than usual. This statement was particularly true for the detector arrays. Therefore, the integration sequence depended heavily on room temperature alignment, using surrogate detector arrays and optical light (see Figure 2). This approach was possible because the optical train is all reflecting, with the exception of the bandpass filters (which were also replaced with surrogates). To first order, it was expected that the alignment would hold at cryogenic temperatures because the instrument is all aluminum. This assumption was tested by cooling the instrument to 80K and repeating the alignment checks using the surrogate detector arrays. Environmental tests were also conducted prior to installation of the flight detector arrays, and the stability of the optics was confirmed with the surrogate detector array procedure. At the end of these tests, the flight detector arrays were installed; we depended on metrology to place them close enough to the positions of the surrogate detector arrays to preserve the alignment. A limited test of alignment was performed at the full instrument level to confirm that this procedure had been successful.

2.1 INITIAL ALIGNMENT

The initial step in alignment was to confirm the correct placement and tilt of the mirrors in the optical train. The instrument was mounted on a conventional vibration isolation table and it was placed relative to the test apparatus by theodolite measurements. The instrument orientation was transferred to an alignment fiducial mounted so it can be viewed as the instrument is integrated with the SIRTF telescope. Pupil placement was examined by projecting an image of the telescope through the optical trains and confirming that it was properly centered and focused and that there was no vignetting (see Figure 3). The focusing properties of the optics were confirmed (and adjusted if necessary by shimming) by projecting light backwards through the system. To do so, each surrogate detector array carried a small array of LED light sources shining though pinholes (see Figure 2) placed at the expected position of the infrared focal plane. The images of these pinholes were projected by the instrument optics to the nominal position of the telescope focal plane, near the pickoff mirrors. A long working distance microscope was used to examine these images, and they were captured by a CCD for later image analysis. Prior to the assembly of the instrument, it was feared that the diamond turned mirrors might have too much scattering for quantitative image analysis. We developed a test procedure based on Ronchi rulings to allow isolation of the image spatial frequencies critical to the far infrared. However, it was obvious when the images were examined that straightforward encircled energy and similar tests would be adequate.

The requirements on the instrument optics were that they should distort the wavefronts at the wavelength of operation by no more than $\lambda/14$ rms at 24μm and no more than $\lambda/25$ at the other wavelengths, providing nominally diffraction limited performance. This requirement was converted into a requirement on encircled energy in optical light. The results of the encircled energy measurements are shown in Figure 4. Except for two extreme corners of the 24μm array, the requirements were met both at room temperature and cold (see below). The design ray traces had shown that the extreme corners of the 24μm array would only marginally meet the specification, so it was concluded that the alignment provided the expected image quality. A second key parameter is focus; the SIRTF instruments are expected to be parfocal. Figure 5 demonstrates that the instrument is well within the focus specification in the 70μm wide field mode. Similar data at the other wavelengths and modes demonstrated parfocality in all cases. Figure 5 also illustrates our ability to carry out precise alignment with optical light. All the images illustrated are within the nominal permissible focus range, and the center images are substantially better than wavefront errors of $\lambda/25$ rms at the operating wavelength, as can be seen from Figure 4.

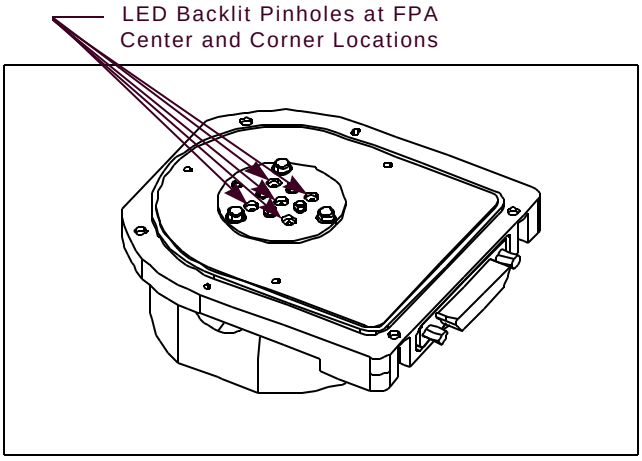

Figure 2. Surrogate for the 24㎜ detector array (compare Figure 1).

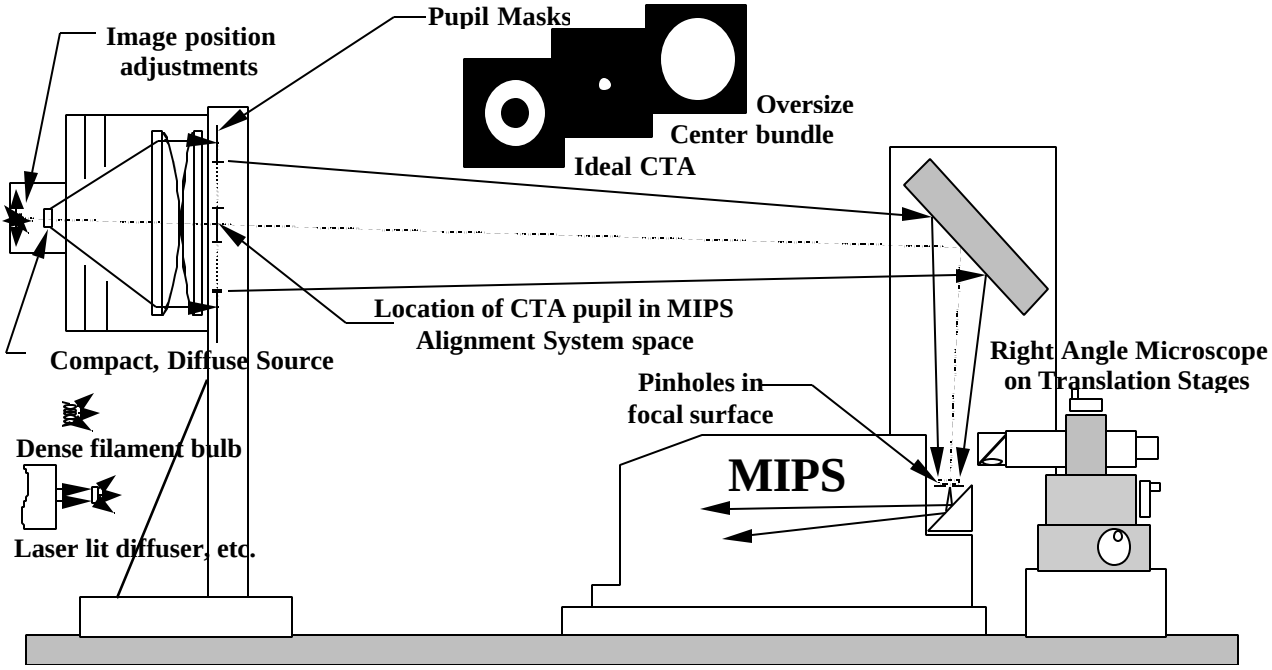

Figure 3. Overall concept for room temperature alignment. The apparatus is shown in the configuration for pupil alignment. If the pinhole sources in the surrogate detector arrays are turned on and the right angle microscope moved into the beam, the imaging properties of the instrument can be characterized.

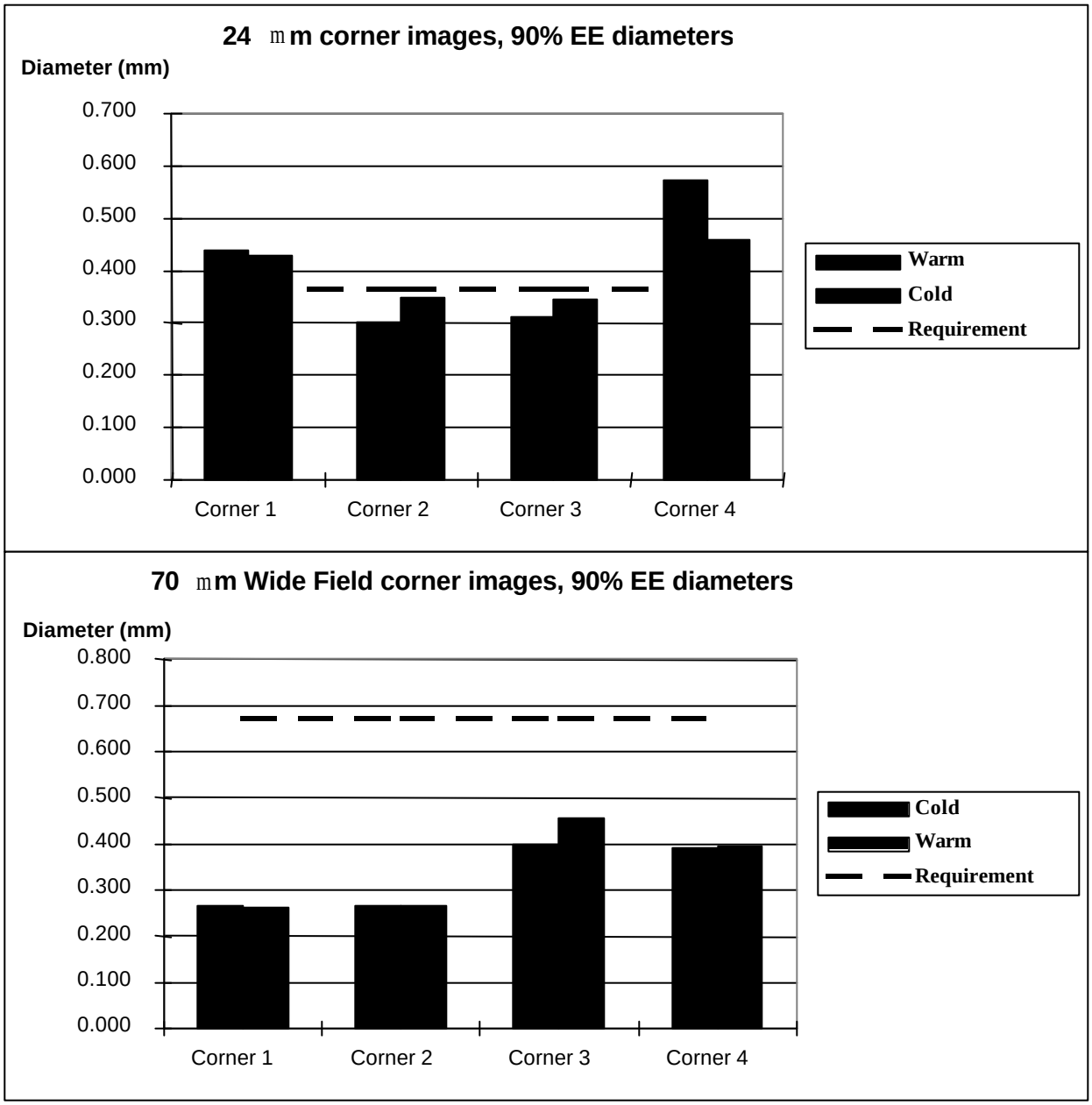

Figure 4. Encircled energy measurements for the extreme corners of the field at 24mm and with the wide field optical train at 70mm. The imaging requirement is l/14 rms at the former wavelength and l/25 rms at the latter.

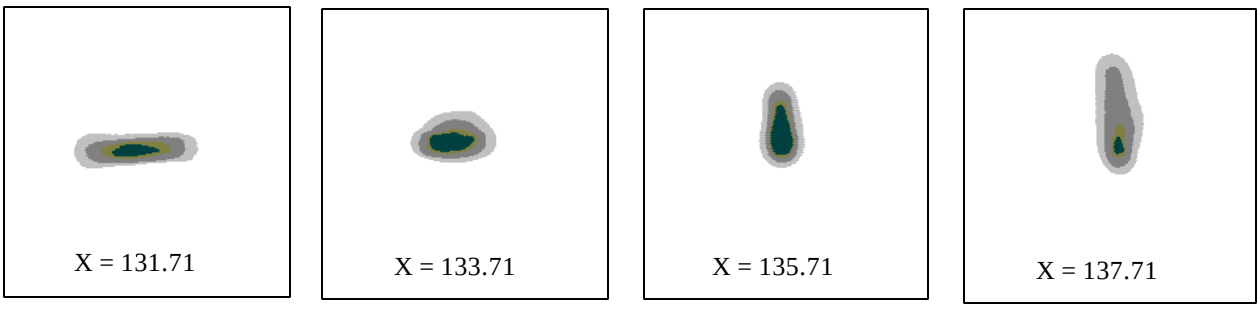

Figure 5. 70 mm wide field center images, cold, through focus. Ideal X=134.77 mm

2.2 LOW TEMPERATURE AND ENVIRONMENTAL TESTING

The next step was to measure any shifts in alignment between room temperature and the temperature of operation. Because nearly all the dimensional change in aluminum occurs between room temperature and 80K, we made the measurements with the instrument cooled with liquid nitrogen. Cooling to a lower temperature would have been much more difficult, with little benefit. The instrument was mounted inside a liquid nitrogen cryostat on an alignment fixture provided by the SIRTF telescope team to simulate the final mounting arrangement. The cryostat was equipped with a window over the instrument pickoff mirrors, through which we made optical measurements. Theodolites were used to reference the alignment fiducial on the instrument to an alignment reference cube on this fixture. The instrument alignment was confirmed with the long working distance microscope by examining the images of the surrogate detector array sources, exactly as when the instrument was under initial alignment. Telescopes were used to locate the Lyot stop in the reference frame of the instrument alignment fiducial. The instrument was then cooled, and the measurements were all repeated. No significant changes were found (see Figure 4) except for a small focus change in the 24μm optical train. Even in this case, both the predicted and the measured positions were within the allowable focus range, but it was decided to make the small adjustment to compensate for the shift at low temperatures.

The instrument was warmed up and its alignment was confirmed with the apparatus on the vibration isolation table. It was then mounted in the vibration cryostat (identical to the one used for checking cold alignment, but with a different vacuum dome that did not have a window). It was cooled to liquid nitrogen temperature, vibrated to the specified protoflight level in all three axes, and warmed up. The alignment was checked again on the vibration isolation table and found not to have changed. These steps completed the integration of the optical system, and it was now ready for the flight detector arrays and bandpass filters.

3. FILTERS AND DETECTOR ARRAYS

3.1 FILTERS

Optical Coating Laboratories, Inc. (OCLI) manufactured the 24μm filter. It is a dielectric stack on a silicon substrate. Because a stack thick enough to provide a bandpass filter would have been at risk for delamination in thermal cycling, MIPS uses a longpass filter and relies on the photoconductive cutoff of the detectors to provide the shortpass part of the band definition. The OCLI filter was traced by the manufacturer, then subjected to vibration testing and thermal cycling, and then traced again. There was no change in transmission properties. The short wavelength blocking of the filter is adequate that even Rayleigh Jeans spectra will have no more than 1% of their net signal from near infrared leaks.

The 70 and 160μm filters were provided by Queen Mary College Industries. The 70μm filters and blockers are capacitive and inductive elements embedded in a hot pressed plastic carrier, while the 160μm filter is on stretched Mylar. Qualification model filters were vibrated at the specified levels. QMCI then repeated their tracings and showed that there was no significant change in transmission properties. The flight filter transmission properties were determined by QMCI, using a series of laboratory spectrophotometers for the wavelength regions visible through far infrared. The blocking by these filters should be adequate that Rayleigh Jeans sources will have no more than 1% of their signal from near infrared leaks. As an example, figure 6 shows on a logarithmic scale the performance of the 70μm filter stack, based on multiplying the transmissions of all the elements measured individually.

3.2 DETECTOR ARRAYS

The 24μm detector array was provided to MIPS by the Infrared Spectrograph (IRS) team. Its manufacturer, Boeing North America, obtained the primary test and qualification data, as summarized in Table 1. BNA also conducted the protoflight vibration testing. Both the 70 and 160μm detector arrays were manufactured at the University of Arizona. The detector arrays were characterized for photometric properties there, see also Table 1. Qualification models were vibrated cold at Ball Aerospace, to qualification levels, and the flight models to protoflight levels, and then retested at the University of Arizona. A failure unrelated to the vibration testing occurred after these tests in the 160μm detector array. The affected module was vibrated to protoflight levels at the University prior to remounting it on the detector array after repair.

Given the strategy of qualifying the instrument optical system and the detector arrays separately, we also conducted an analysis to show that the interface between the two had a very substantial margin of safety.

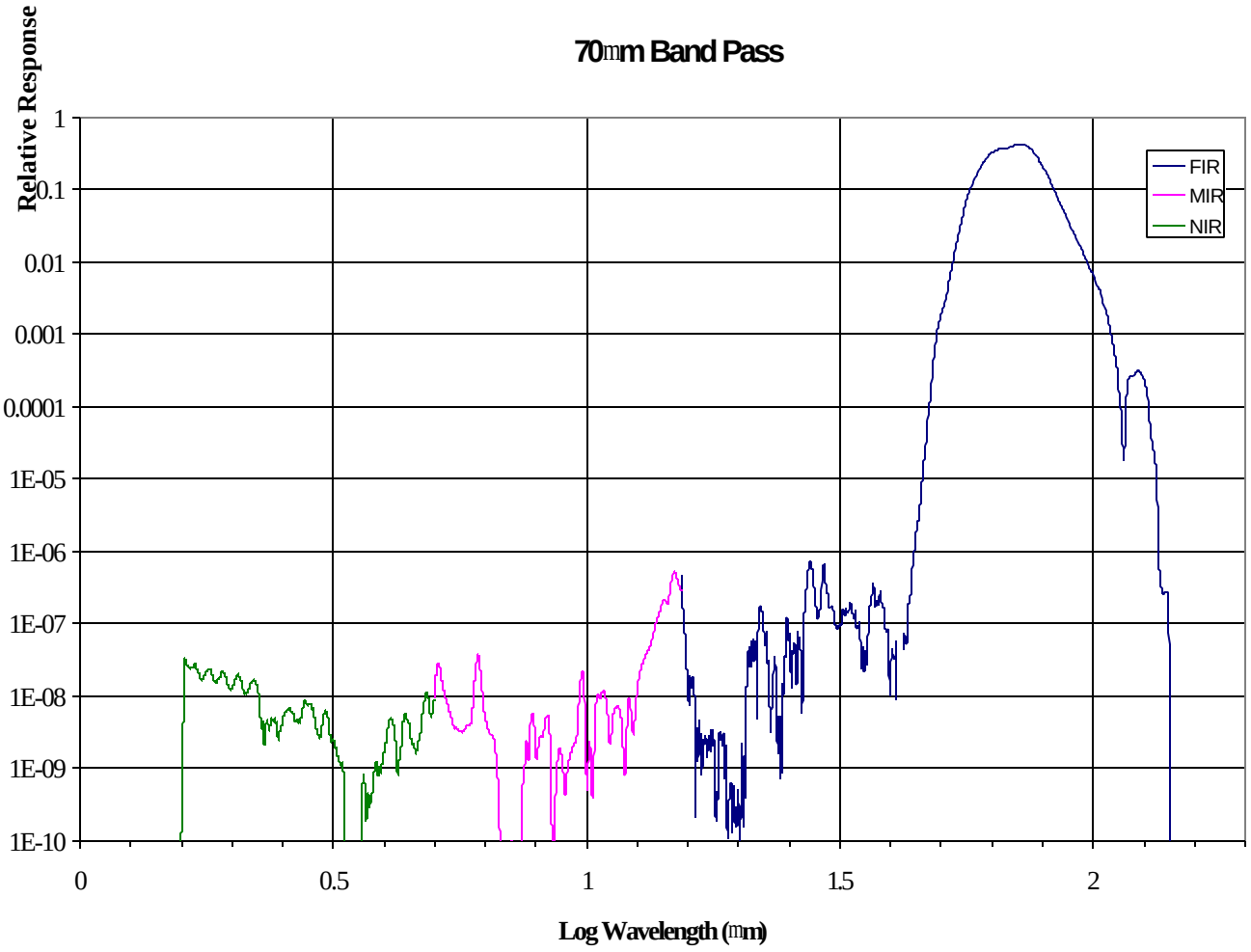

Figure 6. Transmission of the 70μm filter stack. The excellent short wavelength blocking is critical to obtaining good photometry on hot sources such as stars.

Characteristic	24μm Si:As BIB	70μm Ge:Ga	160μm stressed Ge:Ga
Format	128x128	32x32	2x20
Detective Quantum Efficiency*	~ 60%	18%	15%
Responsivity (Amps/Watt)*	---	6.9	13
Departures from Linearity	< 10%	< 4%	< 4%
Interpixel Variability	± 2%	± 40%	± 40%
Spatial Fill Factor	~ 98%	~ 98%	~ 98%
Well Depth (e)	~ 400,000	~ 314,000	~ 410,000
Dark Current (e/s)	~ 3	156	500
Read Noise (e rms)	27	92	248
Radiation Hit Crosstalk	---	< 1%	< 1%
Operability	99.9%	99.6%	100%

* At the indicated wavelength.

Table 1. Detector array characteristics.

4. INTEGRATED INSTRUMENT

The full cold instrument consists of the optical system plus the detector arrays and filters. It was tested in a Low Background Test Cryostat (LBTC), constructed for us by Infrared Laboratories, Inc. The LBTC used a mechanical cooler to cool two radiation shields, one to ~ 150K and the other to ~ 20K. A large helium vessel (10 liters capacity) cooled the instrument and the surrounding baffle box, while a smaller vessel (3 liters) cooled the heat straps to the 70 and 160μm arrays.

The LBTC cooled not only the instrument, but also the apparatus used to inject signals into it, illustrated schematically in Figure 7. This device was a large integrating sphere with an output aperture that covered the telescope focal plane and pickoff mirrors in MIPS. Various reverse bolometer emitters were mounted in its wall to allow injection of signals into the instrument. In addition, pinhole emitters at the focal plane simulated point sources as they would be imaged by the telescope, and also a "sawtooth" shadow mask was placed at one edge of the field to see if the array was being correctly de-multiplexed. The emitters had various fixed bandpass filters to allow testing different aspects of the spectral response of the instrument. The instrument scan mirror shifted the field view between the test fixture features and a position where the entire field of each array was illuminated.

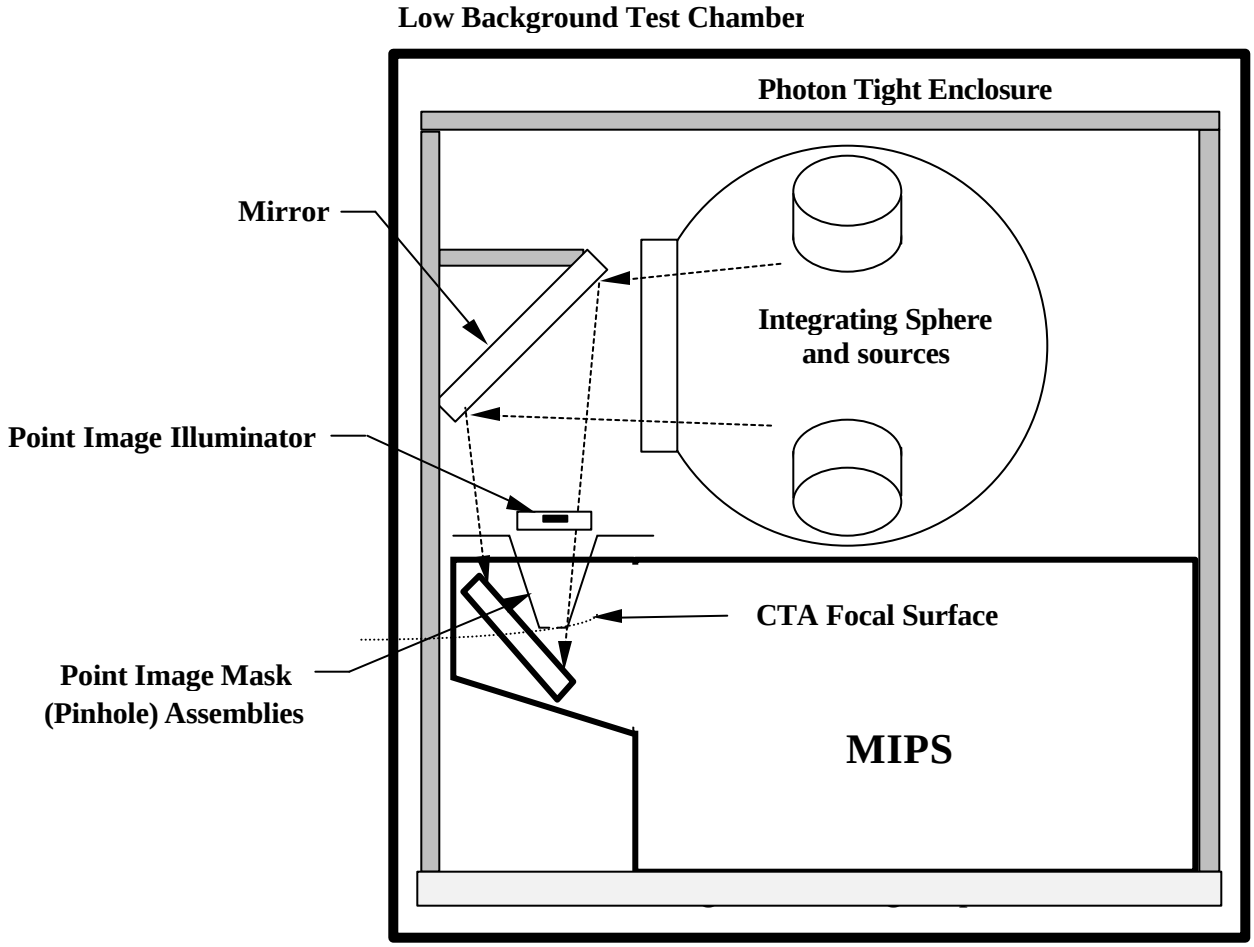

Figure 7. Concept for cryogenic testing of the completed instrument. The cooling and mounting baseplate, along with the photon tight enclosure, are heat sunk to a helium bath that could be pumped to below 2K. The surrounding radiation shield was held near 20K by a mechanical cooler. A separate helium vessel (not shown) provided cooling to below 1.4K through the heat straps to the far infrared detector arrays.

4.1. ENCIRCLED ENERGY

The pinhole sources at the telescope focal plane consisted of a reverse-bolometer thermal emitter in an integrating cavity. The output of this cavity was a long drilled hole with a bend, so that the photons would be thoroughly mixed. The pinhole was placed over the end of this light pipe. All pinholes were sized to a diameter equivalent to one pixel in entry plane space for each band. The Code V instrument model was used to predict the sizes of the pinhole images on the detector arrays.

The Code V model for the 24 and 70μm Wide Field bands takes into acount four factors:

Actual (non-zero) source size
MIPS model aberrations at actual field points
Diffraction at three in-band wavelengths
MIPS model aberrations for actual point defocus

Since it is easy to show that diffraction is the only item of significance in the 160μm band the treatment was limited to its effects alone.

In measuring the pinhole image diameters, the greatest difficulty is determining the zero level, since images affected by diffraction have very large low surface brightness wings. We concentrated our measurements on 60% encircled energy because the effects of the zero level become increasingly greater for larger percentages of encircled energy. In addition, we quote a range of values corresponding to 50 to 60% predicted encircled energy, since for the 24 and 160μm bands the ratios of "100%" image diameter and 60% image diameter as measured were small enough to indicate that the true zero level was overestimated. The results are in the following table.

Wavelength (μm)	Predicted image diameter (pixels)	Measured image diameter (pixels)	Airy disk FWHM (pixels)
24	3.0 to 3.8	2.6	2.4
70 (wide field)	2.2 to 2.6	2.6	1.8
160	3.0 to 3.8	2.6	2.5

Table 2. Encircled energy measurements in the completed cold instrument.

The suspicion that the zero level is overestimated for the 24 and 160μm bands is confirmed since the measured values are at the small end of the range, corresponding to 50% or less encircled energy. The values in all cases show that the imaging is as expected from the more accurate image quality assessment with optical light.

4.2 DETECTOR ARRAY PERFORMANCE

There were various sources of electrical interference in the test setup – the vacuum gauge on the LBTC, the mechanical cooler, etc. In addition, we were unable to connect the grounds in a way that preserved the shielded twisted pair arrangement all the way from the detector arrays to the warm electronics, as will be the case for the flight configuration. Therefore, the noise measurements should be taken as upper limits. The 70μm read noise in 3 seconds was measured at 167 electrons. This value corresponds to 1.24mJy for 5 sigma in 500 seconds for the end to end sensitivity of the array on a point source in SIRTF, within the specification. A noise of 219 electrons was measured with the 160μm array, corresponding to 4.08mJy for 5 sigma in 500 seconds, again better than the specification. With the 24μm array, excess noise appeared to be absent and the read noises for 10 and 20 second integrations were essentially identical to those measured by the manufacturer. This channel should be a factor of at least 1.5 more sensitivie than the specification. All sensitivities use the MIPS radiometric model and include flat fielding noise, which was not included in the original sensitivity estimates.

4.3 INTERNAL STIMULATOR PERFORMANCE

Figure 8 shows the standard deviations over the 70μm array from comparison of signals from repeated flashes of the MIPS internal flood stimulator. A series of seven flashes has been analyzed. For each pixel, the data were de-trended by a linear fit to the signals. Then, a running average of two pixels was taken over the residuals to this fit. Standard deviations were computed on a per-pixel basis over the resulting six samples, with results indicated in the figure. In the

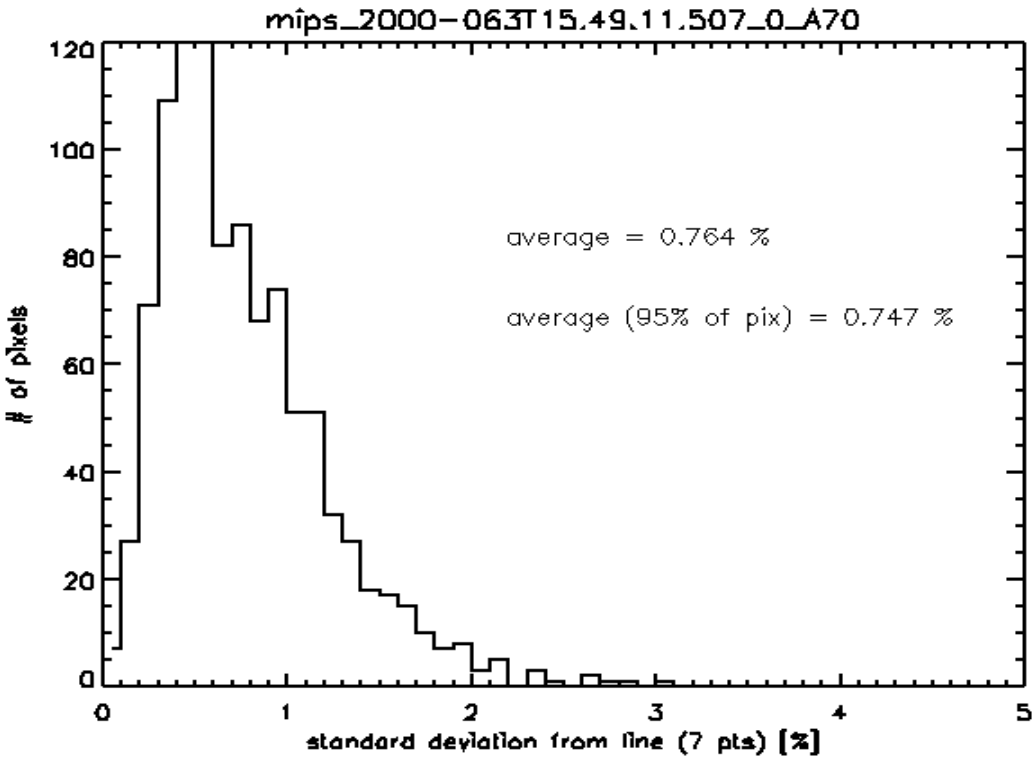

Figure 8. Distribution of observed flat fielding noise, 70μm.

calculation, we allowed for the two degrees of freedom taken by the detrending. The distribution plot shows that the flat fielding noise is well behaved.

These data include fewer points than would normally be used to obtain an accurate estimate of the standard deviation. Averaging the 1000 pixels removes the problem in terms of a stable final result, but there will be more scatter (noise on the noise) than would have been the case if we had used data with many more points. As a result, the distribution in the figure is made artificially broad. To determine the extent of this effect, we used a Monte Carlo program in which we could vary the number of samples used in determining the standard deviation. We compared 6 samples with 100 samples, assuming that 100 was a large enough value that the "noisiness" of the noise estimate was small. In both cases we averaged 1000 cases to provide a similar situation to the averaging on our 32x32 array. The result was that the standard deviation is overestimated by 17% in the calculation with only 6 samples. We conclude that the true standard deviation in the flat fielding with the flood stimulator is 0.76/1.17 = 0.65%. Finally, we correct this value for shot noise, assuming a typical level of half full well. The resulting intrinsic noise in the flat fielding is 0.60%. Slightly more sophisticated approaches to fitting the data have demonstrated stimulator signal repeatability to better than 0.4%, and we conclude that the stimulators can be taken to track the array response very accurately. This conclusion is fundamental for the MIPS data pipeline.

A large gradient was found in the illumination pattern for the 160μm array with its flat fielding stimulators. This effect arises because the light pipe used to inject the stimulator signals penetrates a mirror at an angle of 45 degrees, causing diffraction that skews the output illumination pattern. Nonetheless, the flat fielding performance on the 160μm array is similar to that at 70μm. For the 24μm array, stimulator flashes repeated to the 0.25 – 0.5% level, indicating that flat fielding to 1% is not a significant issue. This result is expected because the detector architecture in this array avoids many of the complications in response characteristics of the bulk photoconductors at 70 and 160μm.

4.4 SPECTROMETER CALIBRATION

The wavelength calibration of the spectrometer was determined by measuring the spectrum of a filter in the pinhole stimulator. We predicted the response from the wavelength dependence of detector response, the grating efficiency, and the measured filter characteristics. The observed spectrum was adjusted in dispersion and wavelength to optimize the fit to the prediction. Figure 9 shows a fit near the values adopted as the final calibration. We concluded that the dispersion is about 1.73μm per pixel, compared with the prediction from the design of 1.68μm/pixel. The difference could arise through a combination of small alignment errors (e.g., off slightly in focus) and measurement error. The fits indicate the shortest wavelength pixel is at 53.35μm.

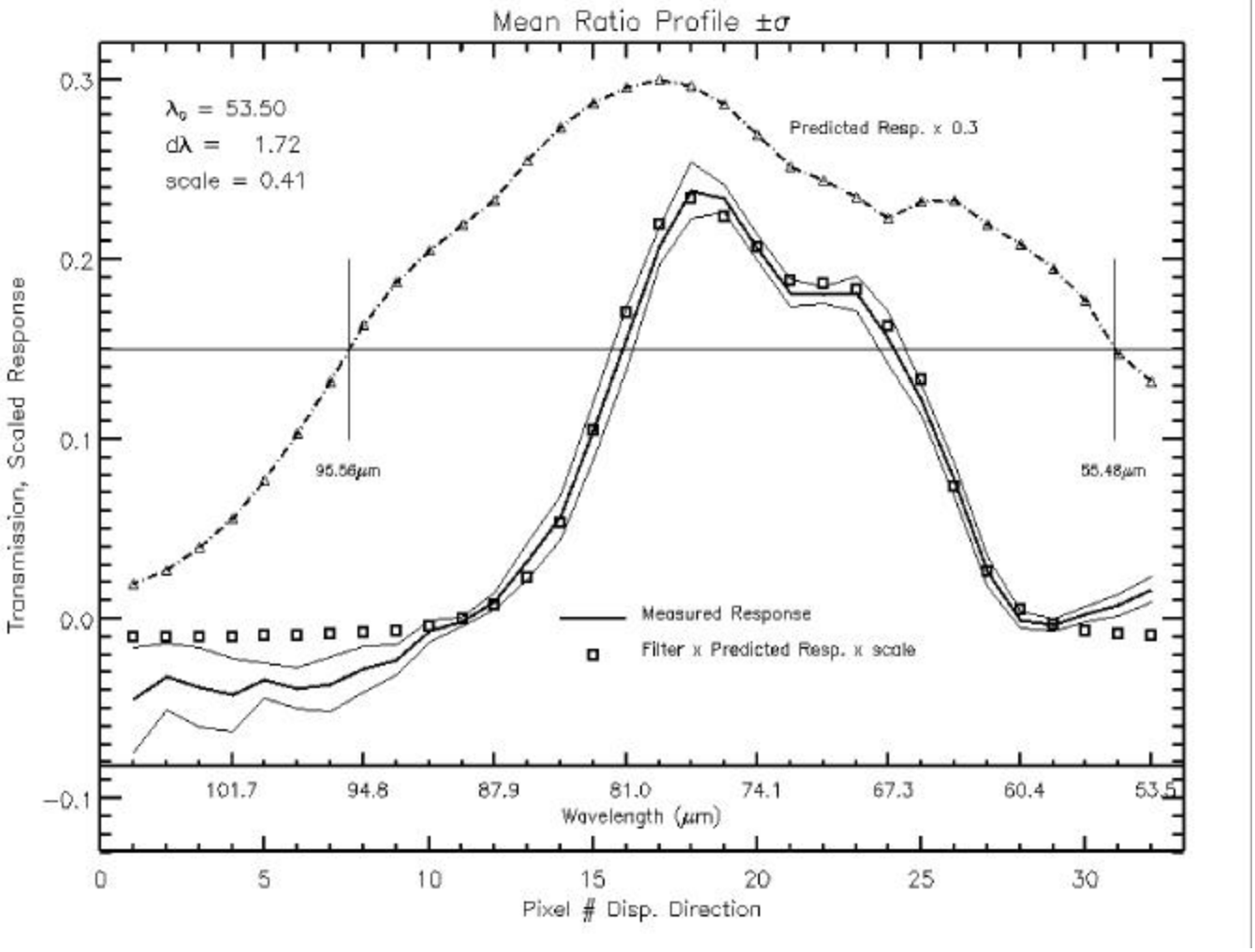

Figure 9. Response of the Spectrometer Mode to a Bandpass Filter. The figure also shows the predicted response of the spectrometer without the filter used for the test.

4.5 OPERABILITY

Once the SIRTF instruments are integrated into the telescope, access to them is essentially impossible. As a result, we put a high priority on testing in as realistic an environment as possible to be sure we had identified and fixed any issues with the instrument operability. We used a full set of flight-like cables to connect the instrument to the warm electronics. The command and data interface with these electronics was always through a simulator of the SIRTF spacecraft electronics, provided by the spacecraft contracter Lockheed Martin Missile Systems. The control console to the spacecraft simulator was provided by JPL to simulate the command environment for the mission. Toward the end of the

test program, the SIRTF Science Center provided a number of command sequences to execute flight-like observing sequences. These sequences were successfullly carried out through the entire string of electronics and instrument.

The flight-like testing environment proved critical in identifying problems. It exposed a number of issues with detector array grounding and with effects on the array control signals caused by the capacitance of the flight-like cabling. Timing misunderstandings in the command sequences became apparent. In addition, by exercising the warm electronics and the control software intensively for four months of testing, many subtle problems were discovered and fixed.

5. SUMMARY

The MIPS was designed to provide orders of magnitude better performance for far infrared astronomy than has been achieved previously. Demonstrating that the instrument satisfied these goals was a challenge, since it required tesging under extremely low far infrared backgrounds as well as confirming the alignment of imaging optics. Furthermore, the schedule and budget for the instrument were very tight. The integration and test plan recognized these challenges by emphasizing thorough measurement of the instrument optical system using visible light, and by adopting a simple (compact, no moving parts) but versatile test apparatus to use in verifying the performance at the integrated instrument level. All the critical instrument functions were thoroughly verified in this way. The instrument has been shown to meet the performance requirements and can be expected to perform up to specification in SIRTF.

6. ACKNOWLEDGEMENTS

SIRTF has had an exceptionally long gestation period between payload selection and construction. As a result, many have contributed to the concept of MIPS, even if the details were never realized. We thank them for their patience as well as their ideas. We also thank the IRS team for leading the development of the common IRS/MIPS electronics and software, and for providing the 24μm array. The current MIPS team, consisting of the project management at JPL as well as the science team, the technical and management personnel at the University of Arizona, and the support effort at Ball Aerospace, worked hard, skillfully, and very smoothly together to make the instrument a reality. The development of MIPS was supported through JPL under contract 960785.

7. REFERENCES

1. G. B. Heim, M. L. Henderson, Kim I. Macfeely, T. J. McMahon, D. Michika, R. J. Pearson, G. H. Rieke, J. P. Schwenker, D. W. Strecker, C. L. Thompson, R. M. Warden, D. A. Wilson, and E. T. Young, "Multiband Imaging Photometer for SIRTF," *SPIE Proceedings* Vol. 3356, 985 - 1000
2. J. van Cleve, T. Herter, R. Butturini, G. Gull, J. R. Houck, B. Pirger, J. Schoenwald, "Evaluation of Si:As and Si:Sb Blocked Impurity Band Detectors for SIRTF and WIRE," *SPIE Proceedings* Vol 2553, May, 1995, 502-513
3. E. T. Young, J. T. Davis, C. L. Thompson, G. H. Rieke, G. Rivlis, R. Schurr, J. Cadien, L. Davidson, G. S. Winters, and K. A. Kormos, "Far-infrared Imaging Array for SIRTF," *SPIE Proceedings* Vol 3354, 57-65
4. R. Schnurr, C. L. Thompson, J. T. Davis, J. W. Beeman, J. Cadien, E. T. Young, E. E. Haller, and G. H. Rieke, "Design of the Stressed Ge:Ga Far-infrared Array for SIRTF," *SPIE Proceedings* Vol 3354, 322-331
5. R. M. Warden and Gerald B. Heim, "Cryogenic Scan Mirror Mechanism for SIRTF/MIPS," 32nd Aerospace Mechanisms Symposium, May 1998